Vol 18 No 8, August 2009
1674-1056/2009/18(08)/3431-07

Chinese Physics B

© 2009 Chin. Phys. Soc.
and IOP Publishing Ltd

Study of MPI based on parallel MOM on PC clusters for EM-beam scattering by 2-D PEC rough surfaces*

Ma Jun(麻 军)†, Guo Li-Xin(郭立新), and Wang An-Qi(王安琪)

School of Science, Xidian University, Xi'an 710071, *China*

(Received 30 December 2008; revised manuscript received 13 February 2009)

This paper firstly applies the finite impulse response filter (FIR) theory combined with the fast Fourier transform (FFT) method to generate two-dimensional Gaussian rough surface. Using the electric field integral equation (EFIE), it introduces the method of moment (MOM) with RWG vector basis function and Galerkin's method to investigate the electromagnetic beam scattering by a two-dimensional PEC Gaussian rough surface on personal computer (PC) clusters. The details of the parallel conjugate gradient method (CGM) for solving the matrix equation are also presented and the numerical simulations are obtained through the message passing interface (MPI) platform on the PC clusters. It finds significantly that the parallel MOM supplies a novel technique for solving a two-dimensional rough surface electromagnetic-scattering problem. The influences of the root-mean-square height, the correlation length and the polarization on the beam scattering characteristics by two-dimensional PEC Gaussian rough surfaces are finally discussed.

Keywords: electromagnetic scattering, rough surface, beam, parallel computing
PACC: 4120, 4110H

1. Introduction

The study of electromagnetic scattering by rough surfaces has been the subject of intensive investigations for its applications in a number of important research areas such as the measurement of the sea wind field and the remote sensing of soil humidity.[1,2] The analytical methods such as the Kirchhoff approximation (KA)[3] and the Small Perturbation Method (SPM)[4] have played a very dominant role over the past several decades. Due to their rigid limitations and low precisions, the study of the exact solution of Maxwell equations for rough surface scattering through numerical methods becomes more and more necessary. In this paper, the method of moment (MOM) with RWG vector basis function and Galerkin's method for calculating electromagnetic beam scattering by two-dimensional (2-D) PEC Gaussian rough surfaces are introduced. But the 3-D vector wave scattering problem presents a great computational challenge by the fact that the MOM generates a dense matrix, even moderately sized electric problems can require a very large number of unknowns. In order to solve this large scale linear equation, Rokhlin V and Chew W *et al* have developed the Fast Multipole Method (FMM)[5,6] and the parallel Multilevel Fast Mutipole Method (MLFMM)[7,8] to reduce the complexity of the matrix-vector multiplication to $O(N \log N)$ which have been used to solve scattering problems from electrically large objects. The Sparse Matrix Canonical Grid (SMCG) and its parallel multilevel expansion[9,10] are investigated to study the electromagnetic (EM) scattering from 2-D large scale dielectric rough surfaces by Tsang L *et al*. Different from these fast numerical algorithms, because the low cost of the parallel computing platform based on the personal computer (PC) clusters makes its application for calculating electromagnetic scattering more and more popular,[11] the parallel MOM is investigated to solve electromagnetic beam scattering from a 2-D PEC Gaussian rough surface by parallel MOM based on the message passing interface (MPI) of PC clusters in this paper. Although the parallel MOM was exploited to study the performance of the multiple antennas mounted on complex platforms,[12] it is firstly investigated to research the EM scattering by rough surfaces in this work.

The 2-D Gaussian rough surfaces are generated by finite impulse response filter (FIRF) theory combined with the fast Fourier transform (FFT) method,[13]

*Project supported by the National Natural Science Foundation of China (Grant No 60571058) and the Specialized Research Fund for the Doctoral Program of Higher Education, China (Grant No 20070701010).
†Corresponding author. E-mail: clack2006@163.com

and then fitted by the triangle patches. Electric field integral equations (EFIE) are discretized by using the RWG vector basis functions[14] and Galerkin's method. Finally, the electromagnetic beam scattering characteristic by a 2-D PEC Gaussian rough surface is investigated on the PC clusters.

2. Parallel MOM based on PC clusters for calculating 2-D rough surface scattering

2.1. Modeling of the two-dimensional Gaussian rough surface

Let the height function of the 2-D Gaussian rough surface be $z(\boldsymbol{r}_s)$, where $\boldsymbol{r}_s = (x, y)$. The statistical characteristics of the Gaussian rough surfaces are defined by the properties[15,16]

$$E(z(\boldsymbol{r}_s)) = 0, \tag{1}$$

$$E\left(z\left(\boldsymbol{r}_s\right) z\left(\boldsymbol{r}_s'\right)\right) = \sigma^2 \exp(-\left|\boldsymbol{r}_s - \boldsymbol{r}_s'\right|^2 / l^2). \tag{2}$$

In the above equations, $E\left(\cdot\right)$ denotes the average over the ensemble of realizations. The parameter σ is the root-mean-square surface height, and l is the transverse correlation length of the 2-D Gaussian rough surface. Here, the 2-D Gaussian rough surface is generated by the FIRF theory combined with the FFT method.[13] First, working on a discrete mesh of points in the x–y plane, we generate the uncorrelated Gaussian random surface distribution $z_u\left(\boldsymbol{r}_s\right)$, which has the properties[16] as follows:

$$E\left(z_u\left(\boldsymbol{r}_s\right)\right) = 0, \tag{3}$$

$$E\left(z_u\left(\boldsymbol{r}_s\right) z_u\left(\boldsymbol{r}_s'\right)\right) = \sigma^2 \delta\left(\boldsymbol{r}_s - \boldsymbol{r}_s'\right). \tag{4}$$

The Gaussian rough surface can be generated through convolving with the Gaussian filter function

$$z\left(\boldsymbol{r}_s\right) = \int_{-\infty}^{\infty} \int_{-\infty}^{\infty} F\left(\boldsymbol{r}_s - \boldsymbol{r}_s'\right) \times z_u\left(\boldsymbol{r}_s'\right) \mathrm{d}\boldsymbol{r}_s' \tag{5}$$

where[13]

$$F\left(\boldsymbol{r}_s\right) = \frac{1}{\sqrt{\pi}\left(\dfrac{l}{2}\right)} \exp\left[-\left|\boldsymbol{r}_s\right|^2 / \left(l^2/2\right)\right] \tag{6}$$

In practice, equation (5) is implemented by the FFT method using the discrete grid of the surface points mentioned above and the edge length of the rough surface will be denoted by L. Figure 1 shows a 2-D rough surface, in which $\sigma = 0.1\lambda$, $l = 1.0\lambda$, $L = 8.0\lambda$ and there are 8 discrete points per λ.

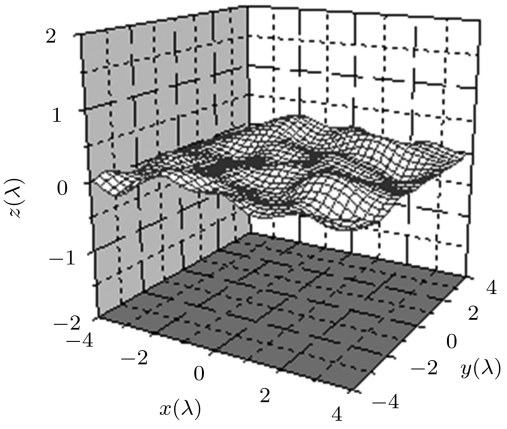


Fig.1. Geometry of a 2-D Gaussian rough surface.

2.2. Electric field integral equation and its discretization

Suppose an incident electric field $\boldsymbol{E}^{\mathrm{inc}}\left(\boldsymbol{r}\right)$ impinging on a 2-D PEC rough surface, based on the fact that the total tangential electric field must vanish on the conducting surface, the EFIE can be written as follows for unknown surface current density $\boldsymbol{J}(\boldsymbol{r})$

$$\hat{\boldsymbol{n}} \times \boldsymbol{E}^{\mathrm{inc}}\left(\boldsymbol{r}\right) = \hat{\boldsymbol{n}} \times \left[jk_0\eta \int_S \boldsymbol{J}(\boldsymbol{r}')G(\boldsymbol{r}, \boldsymbol{r}') + \frac{1}{k_0^2}\nabla' \cdot \boldsymbol{J}(\boldsymbol{r}')\nabla G(\boldsymbol{r}, \boldsymbol{r}')\right] \mathrm{d}s', \tag{7}$$

where $\hat{\boldsymbol{n}}$ is the unit normal vector of the rough surface, k_0 is the free space wave-number, η_0 is the wave impedance of free space, $G(\boldsymbol{r}, \boldsymbol{r}')$ is Green's function

$$G(\boldsymbol{r}, \boldsymbol{r}') = \frac{\exp(-jk_0R)}{4\pi R} = \frac{\exp(-jk_0\left|\boldsymbol{r} - \boldsymbol{r}'\right|)}{4\pi\left|\boldsymbol{r} - \boldsymbol{r}'\right|}. \tag{8}$$

Implementing the RWG vector basis function[14] and Galerkin's method by projecting the triangular elements into the canonical grid as shown in Fig.2, the matrix equation

$$\boldsymbol{Z} \cdot \bar{I} = \bar{V} \tag{9}$$

can then be obtained, where $\boldsymbol{Z}$ is the impedance matrix, $\bar{I}$ the unknown current vector, $\bar{V}$ the voltage vector.

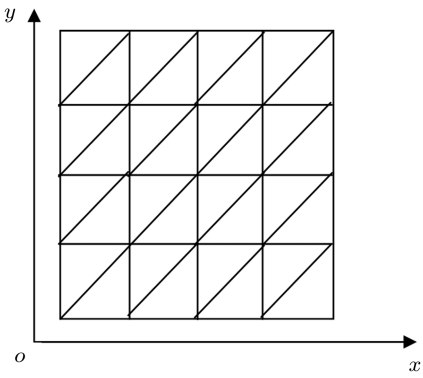


Fig.2. The projection of the rough surface on the x–y plane.

2.3. Introduction of MPI

In the past few years, the computational power of commodity PCs has been doubling about every eighteen months. Meanwhile, network interconnects which provide very low latency and very high bandwidth are also emerging. This trend makes it promising to build high performance computing by clustering, which combines the computational power of commodity PCs and the communication performance of high speed network interconnects.

In this work, the parallel numerical simulations are experimented through PC clusters. A typical parallel computing PC cluster system is composed of several PCs and a high speed interconnect which are used to establish a small-scale local area network as presented in Fig.3.

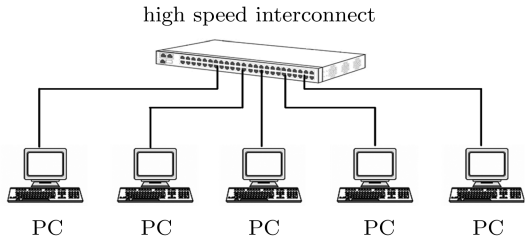


Fig.3. The composition of the PC clusters.

There are many prominent advantages to conduct parallel computing on PC clusters, for example smaller investment, easier programming, more flexible architecture, higher cost-effective, more scalability in comparison with the expensive supercomputers and appropriative parallel computer systems.

The main configuration of clusters in this research is as follows.

1) System composing: 8 PCs;

2) For each PC CPU: Intel Pentium 4, 2.4 GHz; Memory: 1 GB; Main-board: ASUS P5KSE;

3) Switch: TP-Link TL-R402M 1000 M;

4) Operation: Windows XP;

5) Programming environment: MPICH2，Visual Fortran.

The MPI[11,17] is a language-independent communications protocol used to program parallel computers, in which both point-to-point and collective communication are supported. The MPI's goals are high performance, scalability, and portability and it remains the dominant model used in high-performance computing today. MPI is not sanctioned by any major standards body; nevertheless, it has become a de facto standard for communication among processes that model a parallel program running on a distributed memory system. Actual distributed memory supercomputers such as computer clusters often run these programs. Based on the above advantages, we adopt MPICH 2.103 to construct the MPI platform on the PC Clusters in this research.

2.4. Conjugate gradient method and its parallelization

In this paper, the CGM[18] is parallelized to solve the matrix equation according to the property of MPI, in which the impedance matrix is divided by lines for different processes involved in the parallel computing system. For a general nonsingular complex matrix equation shown below

$$\boldsymbol{A} \cdot \bar{\boldsymbol{x}} = \bar{b}, \tag{10}$$

we use CGM to solve the equation as in the procedure given in Fig.4, where $\langle\cdot\rangle$ and $\|\cdot\|$ stand for the inner space product and the norm number, respectively. For two vectors $\bar{x} = [x_1, x_2, \ldots, x_n]^{\mathrm{T}}$, $\bar{y} = [y_1, y_2, \ldots, y_n]^{\mathrm{T}}$, $\langle \bar{x}, \bar{y} \rangle = \sum_{i=1}^{n} x_i y_i^*$, $\|\bar{x}\| = \sqrt{\langle \bar{x}, \bar{x} \rangle} = \sqrt{\sum_{i=1}^{n} |x_i|^2}$, superscripts "*" and "+" denote conjugate and associate respectively. In Fig.4 ε is the residual, and here we choose $\varepsilon = 0.001$.

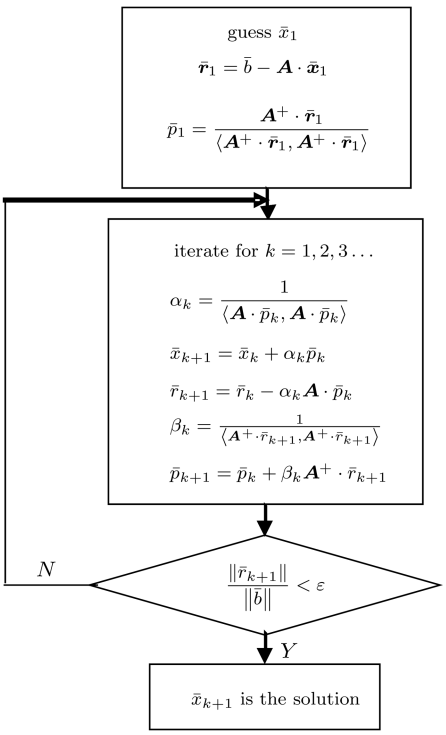


Fig.4. The procedure of the conjugate gradient method.

With the purpose of making each process involved in the paralleling computing system have a balanceable task, the whole impedance matrix must be divided averagely. According to the properties of the MPI, the matrix is divided by lines or rows for different processes in this paper. In the CGM, the product $\boldsymbol{A}\cdot\bar{\boldsymbol{x}}$ of the matrix $\boldsymbol{A}$ and a vector $\bar{\boldsymbol{x}}$, the product $\boldsymbol{A}^+\cdot\bar{\boldsymbol{x}}$ of the matrix $\boldsymbol{A}^+$ and a vector $\bar{\boldsymbol{x}}$ must be computed, which is a critical step to realize the two products on the parallel system, where $\boldsymbol{A}^+$ is the associated matrix of $\boldsymbol{A}$. Here, we take the 8×8 matrix shown in Figs.5(a) and 5(b) as an example. The first subscript of the matrix's and vector's elements denotes the number of the processes where the elements are stored.

$$\begin{bmatrix} a_{01} & a_{02} & a_{03} & a_{04} & a_{05} & a_{06} & a_{07} & a_{08} \\ a_{11} & a_{12} & a_{13} & a_{14} & a_{15} & a_{16} & a_{17} & a_{18} \\ a_{21} & a_{22} & a_{23} & a_{24} & a_{25} & a_{26} & a_{27} & a_{28} \\ a_{31} & a_{32} & a_{33} & a_{34} & a_{35} & a_{36} & a_{37} & a_{38} \\ a_{41} & a_{42} & a_{43} & a_{44} & a_{45} & a_{46} & a_{47} & a_{48} \\ a_{51} & a_{52} & a_{53} & a_{54} & a_{55} & a_{56} & a_{57} & a_{58} \\ a_{61} & a_{62} & a_{63} & a_{64} & a_{65} & a_{66} & a_{67} & a_{68} \\ a_{71} & a_{72} & a_{73} & a_{74} & a_{75} & a_{76} & a_{77} & a_{78} \end{bmatrix} \begin{bmatrix} x_{(0-7)1} \\ x_{(0-7)2} \\ x_{(0-7)3} \\ x_{(0-7)4} \\ x_{(0-7)5} \\ x_{(0-7)6} \\ x_{(0-7)7} \\ x_{(0-7)8} \end{bmatrix}$$

Fig.5(a). The product of a matrix and a vector.

$$\begin{bmatrix} a^*_{01} & a^*_{11} & a^*_{21} & a^*_{31} & a^*_{41} & a^*_{51} & a^*_{61} & a^*_{71} \\ a^*_{02} & a^*_{12} & a^*_{22} & a^*_{32} & a^*_{42} & a^*_{52} & a^*_{62} & a^*_{72} \\ a^*_{03} & a^*_{13} & a^*_{23} & a^*_{33} & a^*_{43} & a^*_{53} & a^*_{63} & a^*_{73} \\ a^*_{04} & a^*_{14} & a^*_{24} & a^*_{34} & a^*_{44} & a^*_{54} & a^*_{64} & a^*_{74} \\ a^*_{05} & a^*_{15} & a^*_{25} & a^*_{35} & a^*_{45} & a^*_{55} & a^*_{65} & a^*_{75} \\ a^*_{06} & a^*_{16} & a^*_{26} & a^*_{36} & a^*_{46} & a^*_{56} & a^*_{66} & a^*_{76} \\ a^*_{07} & a^*_{17} & a^*_{27} & a^*_{37} & a^*_{47} & a^*_{57} & a^*_{67} & a^*_{77} \\ a^*_{08} & a^*_{18} & a^*_{28} & a^*_{38} & a^*_{48} & a^*_{58} & a^*_{68} & a^*_{78} \end{bmatrix} \begin{bmatrix} x_{01} \\ x_{12} \\ x_{23} \\ x_{34} \\ x_{45} \\ x_{56} \\ x_{67} \\ x_{78} \end{bmatrix}$$

Fig.5(b). The product of an associated matrix and a vector.

The product of the matrix and the vector:

Process 0: computing $\sum_{i=1}^{8} a_{0i} \times x_{0i} = b_0$, receiving b_j from Process j. The final product $\boldsymbol{A} \cdot \bar{\boldsymbol{x}} = \bar{y} = [b_0\ b_1\ b_2\ b_3\ b_4\ b_5\ b_6\ b_7]^{\mathrm{T}}$.

Process j $(j = 1, \ldots, 7)$: computing $\sum_{i=1}^{8} a_{ji} \times x_{ji} = b_j$, then sending b_j to Process 0.

The product of the associated matrix and the vector:

Process 0: computing $b_{0i} = a^*_{0i} x_{01}$ for $i = 1, \ldots, 8$ to obtain the vector $\bar{c}_0 = [b_{01}\ b_{02}\ b_{03}\ b_{04}\ b_{05}\ b_{06}\ b_{07}\ b_{08}]^{\mathrm{T}}$; receiving vector $\bar{c}_j$ from Process j; computing the final product $\boldsymbol{A}^+ \cdot \bar{\boldsymbol{x}} = \bar{y}' = [y_1\ y_2\ y_3\ y_4\ y_5\ y_6\ y_7\ y_8]^{\mathrm{T}}$, where $y_m = \sum_{k=0}^{7} b_{km}$, $(m = 1, \ldots, 8)$.

Process j $(j = 1, \ldots, 7)$: computing $b_{ji} = a^*_{ji} x_{j(j+1)}$ for $i = 1, \ldots, 8$ obtains the vector $\bar{c}_j = [b_{j1}\ b_{j2}\ b_{j3}\ b_{j4}\ b_{j5}\ b_{j6}\ b_{j7}\ b_{j8}]^{\mathrm{T}}$, sending $\bar{c}_j$ to Process 0.

2.5. The simulation of the tapered incident electromagnetic beam

In order to avoid unwanted edge effects because the rough surface simulated is not infinite, a tapered incident beam must be introduced.[15] Consider an electromagnetic beam impinging on a 2-D rough surface. The incident fields are expanded as a superposition of weighted plane waves.[19,20]

$$\begin{aligned} &\boldsymbol{E}^{\mathrm{inc}}(x, y, z) \\ &= \int_{-\infty}^{\infty} \int_{-\infty}^{\infty} (E_v \hat{\boldsymbol{v}} + E_h \hat{\boldsymbol{h}}) \\ &\quad \times \exp\left[j(-k_x x - k_y y + k_z z)\right] \mathrm{d}k_x \mathrm{d}k_y, \end{aligned} \quad (11)$$

where $\hat{\boldsymbol{h}}$ and $\hat{\boldsymbol{v}}$ indicate the horizontal and vertical polarization directions, respectively, $k_z = \sqrt{k_0^2 - k_\rho^2} =$

$\beta + \mathrm{i}\alpha$, $k_\rho = \sqrt{k_x^2 + k_y^2}$ and

$$\beta = \begin{cases} \sqrt{k_0^2 - k_\rho^2}, & k_\rho \le k_0, \\ 0, & k_\rho > k_0, \end{cases} \tag{12a}$$

$$\alpha = \begin{cases} 0, & k_\rho \le k_0, \\ \sqrt{k_\rho^2 - k_0^2}, & k_\rho > k_0,\ z \ge 0, \\ -\sqrt{k_\rho^2 - k_0^2}, & k_\rho > k_0,\ z < 0, \end{cases} \tag{12b}$$

The two directions of polarizations $\hat{\boldsymbol{h}}$ and $\hat{\boldsymbol{v}}$ are so defined that $\left\{\hat{\boldsymbol{k}}_\beta, \hat{\boldsymbol{v}}, \hat{\boldsymbol{h}}\right\}$ forms an orthonormal system for $\hat{\boldsymbol{k}}_\beta = (k_x\hat{\boldsymbol{x}} + k_y\hat{\boldsymbol{y}} - \beta\hat{\boldsymbol{z}})/k_\beta$, i.e.

$$\hat{\boldsymbol{h}} = \frac{\hat{\boldsymbol{z}} \times \hat{\boldsymbol{\beta}}}{\left|\hat{\boldsymbol{z}} \times \hat{\boldsymbol{\beta}}\right|} = \frac{1}{k_\rho}\left(-k_y\hat{\boldsymbol{x}} + k_x\hat{\boldsymbol{y}}\right), \tag{13}$$

$$\hat{\boldsymbol{v}} = -\frac{\beta}{k_\beta k_\rho}\left(k_x\hat{\boldsymbol{x}} + k_y\hat{\boldsymbol{y}}\right) - \frac{k_\rho}{k_\beta}\hat{\boldsymbol{z}}, \tag{14}$$

$$\hat{\boldsymbol{k}}_\beta = \hat{\boldsymbol{v}} \times \hat{\boldsymbol{h}}, \quad \bar{\bar{\boldsymbol{I}}} = \hat{\boldsymbol{k}}_\beta\hat{\boldsymbol{k}}_\beta + \hat{\boldsymbol{v}}\hat{\boldsymbol{v}} + \hat{\boldsymbol{h}}\hat{\boldsymbol{h}}, \tag{15}$$

where $\bar{\bar{\boldsymbol{I}}}$ is a unit dyad. The amplitude functions E_h and E_v are the components of a Gaussian tapered spectrum,[20]

$$\begin{aligned} &\boldsymbol{E}(k_x, k_y) \\ &= (E_v^i\hat{\boldsymbol{v}}_i + E_h^i\hat{\boldsymbol{h}}_i)\frac{g^2}{4\pi} \\ &\quad \times \exp\left\{-\left[(k_x - k_{ix})^2 + (k_y - k_{iy})^2\right] g^2/4\right\}, \end{aligned} \tag{16}$$

where $k_{ix} = k\sin\theta_i\cos\varphi_i$, $k_{iy} = k\sin\theta_i\sin\varphi_i$, θ_i and φ_i are the center angles of the incident waves; $\hat{\boldsymbol{h}}_i = -\sin\varphi_i\hat{\boldsymbol{x}} + \cos\varphi_i\hat{\boldsymbol{y}}$, $\hat{\boldsymbol{v}}_i = -\cos\theta_i\cos\varphi_i\hat{\boldsymbol{x}} - \cos\theta_i\sin\varphi_i\hat{\boldsymbol{y}} - \sin\theta_i\hat{\boldsymbol{z}}$, E_h^i and E_v^i are the relative amplitudes of the two polarizations. The parameter g controls the tapering of the incident waves and is taken to be $L/5$. Substituting Eqs.(13)–(15) and $E_v(k_x, k_y) = \hat{\boldsymbol{v}} \cdot \boldsymbol{E}(k_x, k_y)$, $E_h(k_x, k_y) = \hat{\boldsymbol{h}} \cdot \boldsymbol{E}(k_x, k_y)$ into Eq.(11), we can compute the incident electric field. The 3-D normalized magnitude of the incident vertical polarized wave on a rough surface with $\sigma = 0.1\lambda$, $l = 1.0\lambda$ and $\theta_i = 20°$, $\varphi_i = 0°$ is shown in Fig.6(a) and its projection in Fig.6(b) respectively.

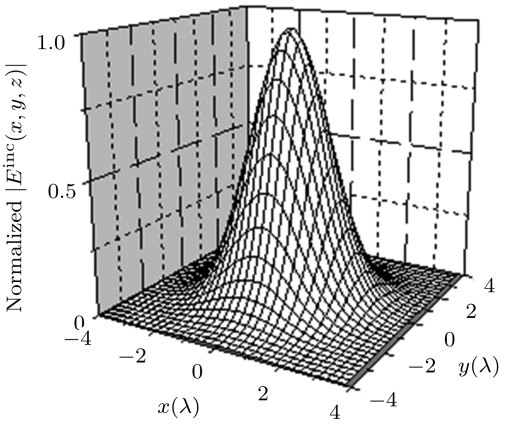


Fig.6(a). Normalized incident field magnitude.

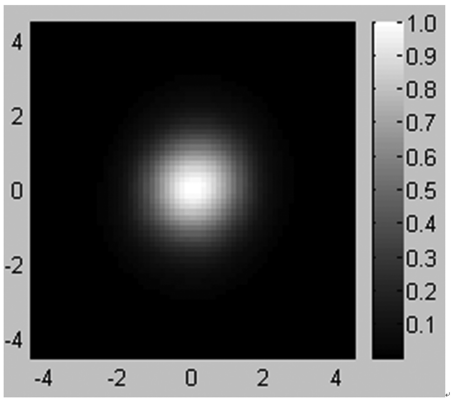


Fig.6(b). The projection of the normalized incident field magnitude.

2.6. The calculating of the scattering field and bistatic scattering coefficients.

Once the surface electric current $\boldsymbol{J}(\boldsymbol{r})$ is solved, the scattered far fields can be calculated by

$$\boldsymbol{E}^s_{r\to\infty} = \left[S_v(\hat{\boldsymbol{k}}_s)\hat{\boldsymbol{v}}_s + S_h(\hat{\boldsymbol{k}}_s)\hat{\boldsymbol{h}}_s\right]\frac{\exp(-jk_0r)}{4\pi r} \tag{17}$$

with

$$S_h(\hat{\boldsymbol{k}}_s) = -jk\eta\hat{\boldsymbol{h}}_s \cdot \int_S \boldsymbol{J}(\boldsymbol{r}')\exp(jk_0\hat{\boldsymbol{k}}_s \cdot \boldsymbol{r}')\mathrm{d}S', \tag{18a}$$

$$S_v(\hat{\boldsymbol{k}}_s) = -jk\eta\hat{\boldsymbol{v}}_s \cdot \int_S \boldsymbol{J}(\boldsymbol{r}')\exp(jk_0\hat{\boldsymbol{k}}_s \cdot \boldsymbol{r}')\mathrm{d}S', \tag{18b}$$

where $\hat{\boldsymbol{k}}_s = \sin\theta_s\cos\varphi_s\hat{\boldsymbol{x}} + \sin\theta_s\sin\varphi_s\hat{\boldsymbol{y}} + \cos\theta_s\hat{\boldsymbol{z}}$ is the scattering direction, $\hat{\boldsymbol{h}}_s$ and $\hat{\boldsymbol{v}}_s$ represent the horizontal and vertical polarization directions respectively,

which are so defined that $\left\{\hat{\boldsymbol{k}}_s, \hat{\boldsymbol{v}}_s, \hat{\boldsymbol{h}}_s\right\}$ forms an orthonormal system,

$$\hat{\boldsymbol{h}}_s = \frac{\hat{\boldsymbol{z}} \times \hat{\boldsymbol{k}}_s}{\left|\hat{\boldsymbol{z}} \times \hat{\boldsymbol{k}}_s\right|} = -\sin\varphi_s \hat{\boldsymbol{x}} + \cos\varphi_s \hat{\boldsymbol{y}}, \tag{19}$$

$$\begin{aligned}\hat{\boldsymbol{v}}_s &= \hat{\boldsymbol{h}}_s \times \hat{\boldsymbol{k}}_s \\ &= \cos\theta_s \cos\varphi_s \hat{\boldsymbol{x}} + \cos\theta_s \sin\varphi_s \hat{\boldsymbol{y}} - \sin\theta_s \hat{\boldsymbol{z}}.\end{aligned} \tag{20}$$

The bistatic scattering coefficient (BSC) is defined as

$$\mathrm{BSC}_{\beta\alpha} = \lim_{r\to\infty} \frac{4\pi r^2}{P^{\mathrm{inc}}} \left|\boldsymbol{E}^s_{\beta\alpha}\right|^2 \quad \alpha, \beta = \mathrm{H}, \mathrm{V}, \tag{21}$$

where P^{inc} is the total power impinged on the surface,[19] α and β are the polarization of the incident wave and scattered wave, respectively.

3. Numerical simulations and discussions

For all the following simulations $L = 9.15\lambda$, $\theta_i = 20°$, $\varphi_i = 0°$ and there are 64 discrete points both along the x and y directions, hence, there are 12160 unknowns which is impossible to solve on one PC.

Firstly, the comparison of computing time for a same surface realization with $\sigma = 0.1\lambda$, $l = 0.5\lambda$ on different numbers of the processes are presented in Table 1. From the table, it is easily found that the accelerator ratio is almost in direct proportion to the numbers of processes involved on the computing parallel system, this indicates that the 2-D rough scattering EM-scattering problem can be solved by this proposed technique.

Table 1. The comparison of computing time for a same surface realization on different numbers of the processors.

number of the processors	filling time/s	solving time/s	total time/s
4 processors	182	440	622
6 processors	121	294	415
8 processors	90	219	309

To explore the electromagnetic beam scattering by the 2-D PEC rough surface, the BSC of different σ, l and polarization are calculated in Fig.7(a) to Fig.8(b) by 15 surface realizations. In Figs.7(a) and 7(b), the influences of σ on the BSC of different polarizations in which $l = 0.5\lambda$ are plotted. For the co-polarization, it is shown that the BSC of HH is larger than that of VV near the specular directions, but for the non-specular direction the BSC of HH is smaller than that of VV.

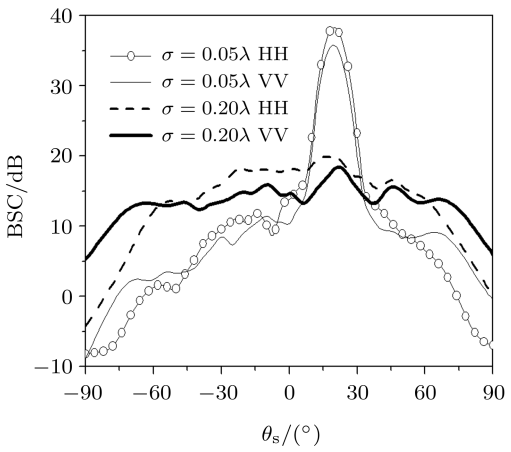


Fig.7(a). Comparison of different σ: co-polarization.

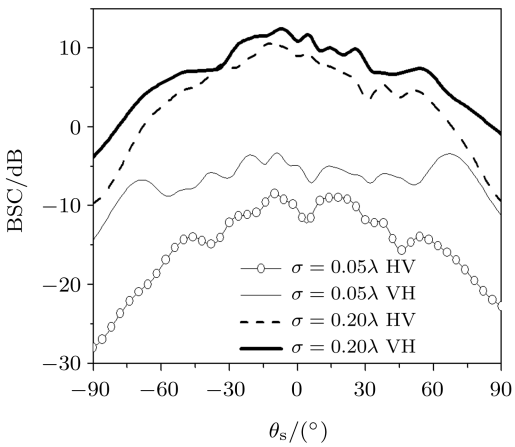


Fig.7(b). Comparison of different σ: cross-polarization.

In addition, with the increase of σ, the BSC near the specular direction (mainly corresponds to the coherent component) decrease, whereas the incoherent component in the non-specular direction increase both for HH and VV. Another point worth noting is that for $\sigma = 0.05\lambda$, the BSC of the co-polarization in the specular direction has a more obvious peak than the result of $\sigma = 0.2\lambda$. As for the cross-polarization concerned, it is observed that the BSC of VH is greater than that of HV for all the scattering angle, and the BSC increases

for both HV and VH with the increasing σ. All these results are due to the fact that the roughness of the Gaussian surface increases with larger σ.

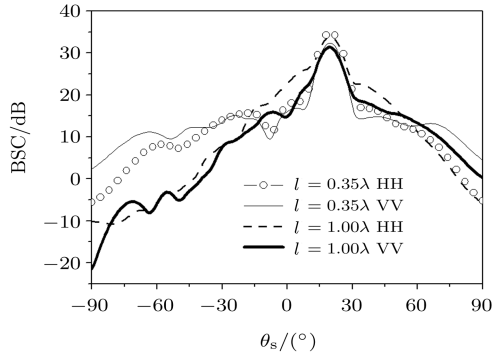


Fig.8(a). Comparison of different l: co-polarization.

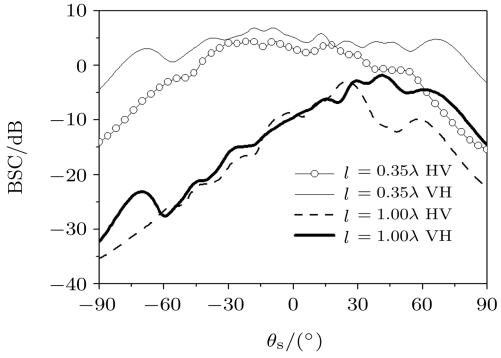


Fig.8(b). Comparison of different l: cross-polarization.

Further illustration of the effect of the correlation length l on the BSC of co-polarization and cross-polarization is presented in Figs.8(a) and 8(b), in which $\sigma = 0.1\lambda$. It is found that the influence of l on the BSC is significant, especially for the non-specular direction for both the co-polarization and the cross-polarization, the primary reason for this is due to the fact that for the smaller l, the height of the Gaussian rough surface varies more heavily, which leads to a more incoherent scattering contribution to the bistatic scattering coefficient in the non-specular direction. As is apparent in Figs.8(a) and 8(b), the larger l, the larger the scattering coefficient will be for the same scattering angle away from the specular direction.

4. Conclusions

To investigate the bistatic scattering characteristics of an electromagnetic beam from a 2-D PEC Gaussian rough surface, the conventional CGM is parallelized according to the properties of the MPI on PC clusters in order to solve the large scale matrix equation generated by MOM. The matrix is divided into different processes by lines for the purpose of making all the processes have a balanced task and being not limited to the hardware of the parallel system. It should be pointed out that although the accelerator ratio equals the numbers of processors involved on the computing parallel system, the size of the rough surface which can be calculated by the parallel MOM is still limited. So the future work is to develop fast and advanced numerical methods combined with parallel computing technology.[5−10] The results of these investigations will appear in future submissions.

References

[1] Ren X C and Guo L X 2008 *Chin. Phys.* B **17** 2956

[2] Wang Y H, Zhang Y M, He M X and Guo L X 2008 *Chin. Phys.* B **17** 3696

[3] Thorsos E I 1988 *J. Acoust. Soc. Am.* **83** 78

[4] Thorsos E I and Jackson D R 1989 *J. Acoust. Soc. Am.* **86** 261

[5] Rokhlin V 1990 *J. Comput. Phys.* **86** 414

[6] Lu C C and Chew W C 1993 *IEE Proceedings-H* **140** 455

[7] Sheng X Q, Jin J M, Song J M, Lu C C and Chew W C 1998 *IEEE Trans. Antennas. Propag.* **46** 1718

[8] Donepudi K, Jin J M, Velamparambil S, Song J M and Chew W C 2001 *IEEE Trans. Antennas. Propag.* **49** 1069

[9] Li S Q, Chan C H and Xia M Y 2001 *IEEE Trans. Antennas. Propag.* **49** 1579

[10] Xia M Y, Chan C H, Li S Q, Zhang B and Tsang L 2003 *IEEE Trans. Antennas. Propag.* **51** 1142

[11] Du Z H 2001 *Programming Technique for High Performance Computation* (Beijing: Tsinghua University Press)

[12] Yu Z, Nan W and Chang H L 2006 *Acta Electron. Sin.* **34** 478

[13] Hu Y Z and Tonder K 1992 *Int. J. Mach. Tools Manufact.* **32** 83

[14] Rao S M, Wilton D R and Glisson A W 1982 *IEEE Trans. Antennas. Propag.* **30** 409

[15] Ogilvy J A 1991 *Theory of Wave Scattering from Random Rough Surface* (Britain: Bristol IOP Publishing)

[16] Robert L, Song J M and Weng C C 1997 *IEEE Trans. Antennas. Propag.* **45** 235

[17] Lauria M and Chien A 1997 *Journal of Parallel and Distributed Computing* **40** 4

[18] Hestenes M and Stiefel E 1952 *J. Res. Nat. Bur. Stand.* **49** 409

[19] Braunisch H, Zhang Y and Chi A 2000*IEEE Trans. Antennas. Propag.* **48** 1086

[20] Xia M Y, Chi H Chan and Shu Q L 2001*IEEE Trans. Geosci. Remote Sensing.* **39** 718